ACTA BIOMATERIALIA ODONTOLOGICA SCANDINAVICA

http://informahealthcare.com/abo
ISSN: 2333-7931 (electronic)

Acta Biomater Odontol Scand, 2015; 1(1): 22–28

informa healthcare

ORIGINAL ARTICLE

Influence of peak oral temperatures on veneer–core interface stress state

Massimo Marrelli[1], Antonella Pujia[2], Davide Apicella[1], Salvatore Sansalone[1], and Marco Tatullo[1,3]

[1]Calabrodental Clinic, [2]Tecnologica, Prosthesis Division, and [3]Tecnologica Research Institute, Biomedical Unit, St. E. Fermi, Crotone, Italy

Abstract

Objective: There is a growing interest for the use of Y-TZP zirconia as core material in veneered all-ceramic prostheses. The objective of this study was to evaluate the influence of CET on the stress distribution of a porcelain layered to zirconia core single crowns by finite elements analysis.
Material and methods: CET of eight different porcelains was considered during the analysis.
Results: Results of this study indicated that the mismatch in CET between the veneering porcelain and the Y-TZP zirconia core has to be minimum (0.5–1 μm/mK) so as to decrease the growing of residual stresses which could bring chipping.
Conclusions: The stress state due to temperature variation should be carefully taken into consideration while studying the effect of mechanical load on zirconia core crown by FEA. The interfacial stress state can be increased by temperature variation up to 20% with respect to the relative failure parameter (interface strength in this case). This means that stress due to mechanical load combined to temperature variation-induced stress can lead porcelain veneer–zirconia core interfaces to failure.

Keywords

FEM analysis, thermal stress, Y-TZP zirconia

History

Received 9 October 2014
Revised 22 March 2015
Accepted 31 March 2015
Published online 29 April 2015

Introduction

The increasing aesthetic demand lead to the manufacturing of prosthetic crowns made up of ceramic cores with layered porcelain veneers.[1] Such types of restorations were introduced to improve biocompatibility and aesthetic of dental prosthetic crowns with respect to conventional metal core crowns.[2–6] The veneers consist of a glass and a crystalline phase of fluoroapatite, aluminum oxide or leucite.[2] The core is commonly made up of leucite or lithium disilicate [7–9] in a glass matrix, diopside or zirconium oxide.[10–20] Zirconium oxide was introduced as core material for all the ceramic restorations due to its chemical and dimensional stability, high mechanical strength and toughness as well as a Young's modulus similar to that of stainless steel.[21] In particular, Yttria-tetragonal-zirconia-polycrystal (Y-TZP) frameworks provide enhanced mechanical strength[22–25] and biocompatibility.[26,27] Accordingly, it is expected that zirconia-core crowns have an occlusal load-bearing capacity[22] suitable for clinical use and represent an alternative to metal-core crowns. The clinical performances of conventionally luted metal-ceramic and zirconia molar crowns and veneering porcelain do not significantly differ in survival, success and ceramic fracture rates.[28] The high strength and fracture toughness of zirconia have supported its extensive application in esthetic dentistry. However, the fracturing of veneering porcelains remains as one of the primary causes of failure.[29] Veneering porcelain chipping is often observed in metal-free crowns.[30–32] The mechanical interface between veneering porcelain and zirconium oxide substructure has been identified as a weak point of metal-free crown.[33] The reliability and longevity of ceramic prostheses have become a major concern. The existing studies have focused on some critical issues from clinical perspectives, but more researches are needed to address fundamental sciences and fabrication issues to ensure the longevity and durability of ceramic prostheses.[34] Thermocycling during fabrication can induce crack nucleation and propagation in porcelain veneered to zirconia core ceramic structures.[35] The veneering process of frameworks induces residual stresses and can initiate cracks when combined with functional stresses. The stress distribution within the veneering ceramic as a function of depth is a key factor influencing failure by chipping. This is a well-known problem with Yttria-tetragonal-zirconia-polycrystal-based fixed partial denture.[36] Mismatch in thermal expansion properties between veneering ceramic and metallic or high-strength ceramic cores can induce residual stresses and initiate cracks when combined with functional stresses. Knowledge of the stress distribution within the veneering ceramic is a key factor for understanding and predicting chipping failures, which are

Correspondence: Dr. Marco Tatullo, PhD, Scientific Director, Tecnologica Research Institute, Biomedical Unit, St. E. Fermi, 88900 Crotone, Italy. Tel: +393498742445. E-mail: marco.tatullo@tecnologicasrl.com

 DOI: 10.3109/23337931.2015.1039536

well-known problems with Yttria-tetragonal-zirconia-polycrystal-based fixed partial dentures.[37] Various experimental and theoretical studies indicate the critical importance of thermal expansion, heat transfer capability of core and veneer on the temperature distributions and residual stresses in zirconia core crown.[35,38] Effect of temperature variation on veneering ceramic and zirconia core stress state due to mismatch in thermal expansion properties had been addressed exclusively by studying and simulating their fabrication thermo-cycling environment. The effect of functional intra-oral temperatures variation on the interfacial stress state of porcelain veneered on zirconia cores has still not been addressed. The aim of the present study is to estimate the stress state induced by thermal dilatation in different porcelain material veneered on Y-TZP core with particular attention to veneer–core interface stresses.

Materials and methods

Finite elements model generation

A metal-free prosthetic crown manufactured to restore a right mandibular molar was sectioned along the frontal plane. The image of the transversal section in lingual to buccal direction was digitalized together with a reference unit of measure. The average thickness of the core ranged from 0.75 to 1.25 mm, while veneer thickness ranged from 0.5 to 2 mm in the cervical area and under the cuspids, respectively. The external profile of the crown, the internal profile of the veneer–core interface and internal profile of the crown core were marked and key-points coordinates were recorded with respect to a reference point. Keypoints coordinates were uploaded in the 2D cad environment of the Finite Elements Analysis software. 2D parametric splines were generated through the keypoints. Two areas were generated from the splines, one representing the veneer cross–section and the other representing the core cross-section. The 2D areas were meshed with four nodes quadrilateral 2D elements with two degrees of freedom per node resulting in a finite elements model (FEM) made-up of 700 elements. The crown FEM is showed in Figure 1 with lines marking the veneer–core interface.

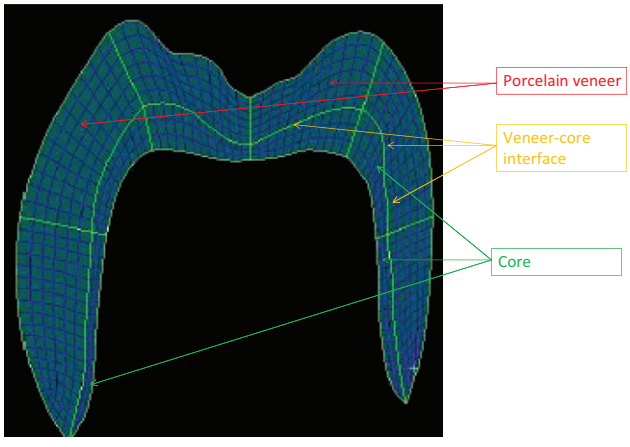

Figure 1. Finite elements model (FEM) of a crown composed by layers of quadrilateral elements simulating the core structure (green arrows) and layers of quadrilateral elements simulating the veneer structure (red arrows), green arrows indicate the veneer–core interface.

Materials properties

Veneering porcelains and YTZ-P core were considered as linear elastic isotropic materials. At this step, eight-crown FEMs were generated by coupling the FEM with the thermal and mechanical properties of eight different veneering porcelains (Table 1). In all the models, the elements simulating the core structure were coupled to the mechanical and thermal properties of YTZ-P (Young's modulus: 201.5 GPa, Poisson's ratio: 0.23 and coefficient of thermal expansion: 10 με/°C).

Boundary conditions

The molar crown was constrained along the internal splines simulating the core surface interfaced with the abutment. A series of nodes were generated close to nodes meshing the internal splines that simulated the core surface interfaced to the abutment. The nodes were generated with a centripetal off-set of ~0.15 mm and connected to core nodes by 2D beam elements. X and Y plane constrains were applied to the off-set nodes. Beam elements connecting the off-set constrained nodes to the core nodes were coupled to the mechanical properties of a luting agent (9.5 GPa, 0.25 ν). A temperature gradient from 75 °C to 0 °C was applied to tested models.

Experimental FEM validations

A mandibular extracted molar was stored in physiological solution for <12 h. It was prepared to obtain a dentine abutment with dimension comparable to those of the generated FE model.

A Y-TZP core was created by CAD-CAM technique. The core was veneered with Triceram according to the veneer thickness simulated in the 2D model. The final crown was cemented by a glass-ionomer cement (RelyX, Luting-plus, 3M-ESPE, St Paul, MN).

The restored molar was embedded in wax and a linear strain gauge (type: C-980204-E, Measurement Group, Inc; Micro-measurements division; Releigh, NC) was bonded on the buccal surface of the restoring crown as shown in Figure 2. The strain gauge is connected to a strain-measuring hardware especially designed for biomedical applications (Omicron-T, Battipaglia, Salerno). A thermocouple was positioned in contact with the crown, close to the strain gauge-measuring

Table 1. Mechanical and thermal properties of simulated veneer materials.

Model	Veneer material	Cet (με/°C)	*E* (Gpa)	Pr
1	Lava Ceram	9.8	71	0.32
2	Ceramco Pfz	9.8	69.2	0.19
3	Vita Vm9	9	65	0.21
4	Triceram	8.9	n.r.	0.25
5	Sakura Interaction	9.7	60	0.265
6	Zirox	8	n.r.	0.22
7	Gc Initial	9.4	65.8	0.17
8	Emax	9.5	65	0.24

The first raw indicate the model simulating the corresponding veneer material. In each model, the core material was coupled to the mechanical properties of Yttria-tetragonal-zirconia-polycrystal.
CET, coefficient of thermal expansion; E, Young's modulus; Pr, Poisson's ratio; n.r., not reported from the company.

area (Figure 2). Cooling and heating systems were set up as follows. The cooling control was achieved by fixing an ethyle chloride bottle by an adjustable mechanical support and by moving the support to vary the distance between the ethyle chloride spry output and the molar crown. The heating control was achieved by fixing a 1600-W hot air plastic welder (Leister, Kagiswill/OW, Switzerland) by an adjustable mechanical support and by moving the support to vary the distance between the hot air plastic welder output and the molar.

The digital temperature-measuring system enables the researcher to adjust the cooling and heating systems in safety conditions by a ''try and error'' approach until an optimal cooling and heating distance was regulated.

During the test, strain gauge signal was first stabilized at room temperature (25 °C), the molar was cooled by opening the ethyle chloride spry to decrease the crown temperature to ~0 °C (Phase A), the cooling gas flux was kept open to maintain the 0 °C temperature for ~10 s (Phase B), the ethyle chloride spry was closed and the molar left exposed to room temperature for ~50 s to enable its spontaneous heating (Phase C). After the molar reached the room temperature, the molar crown was heated to ~75 °C (Phase D) by opening the hot air flux and the heating air flux was kept constant to hold a 75 °C temperature for ~10 s (Phase D). The above-described procedure was repeated 5 times. The crown strain state was recorded as a function of time. According to temperature boundary conditions imposed in the FEA (0–75 °C), the strain state variation between Phase B (0 °C) and Phase D (75 °C) was measured and adopted for FE model validation. The strain state variation was calculated as a mean of the five performed experimental tests. The corresponding stress state was calculated according to Equation (1): $\sigma_y = E/\varepsilon_y$ that is valid for uniaxial stress and strain.

Results

Figure 3 shows a typical strain–time function recorded during a strain-measuring section by strain gauge technique. The light blue line represents the strain state variation during time. The function was divided in five phases (namely: A, B, C, D and E) to better recognize the relative temperature applied to the molar. During cooling (Phase A), strain state decreases in the negative field that stabilizes to approximately −0.0000075 ε (Phase B). The strain-state increase after the cooling flux is interrupted and the sample was left exposed to room temperature (Phase C). During heating (Phase D), the strain state rapidly increases to 0.000014 ε.

For all the tested models, the maximum principal stress and maximum shear stress state were plotted by chromatographic fringes superimposed on the image of 2D models as usually done in FEA results representation. Figure 4 shows maximum principal stress values and distribution for Triceram veneer model.

The higher stress state was estimated along the veneer–core interface, where the stress state ranged from 4.5 to 4.9 MPa. Peak stress of 6 MPa was estimated along the veneer–core interface. Stress progressively decreases toward the boundaries of the models with an exception for the core upper edges, where stress state increases (red arrows in Figure 4). The higher maximum principal stress and maximum shear stress state estimated in each tested model is reported in Table 2.

Discussion

Neglecting the biological variability

One of the main limits of applying FEA to dental biomechanics is the low statistical value of the single ''virtual sample'' being tested. Accordingly, the outcomes of the present investigation should be considered as merely indicative to the setup of further more complex approaches to the problem. However, FE method has chance to become a testing procedure accounting also for biological variability since it can be used with a statistical approach. In this sense, properly experimentally validated 2D FEAs can represent an alternative potential approach to study, in a limited manner, some aspects of the morphological variability characteristic of

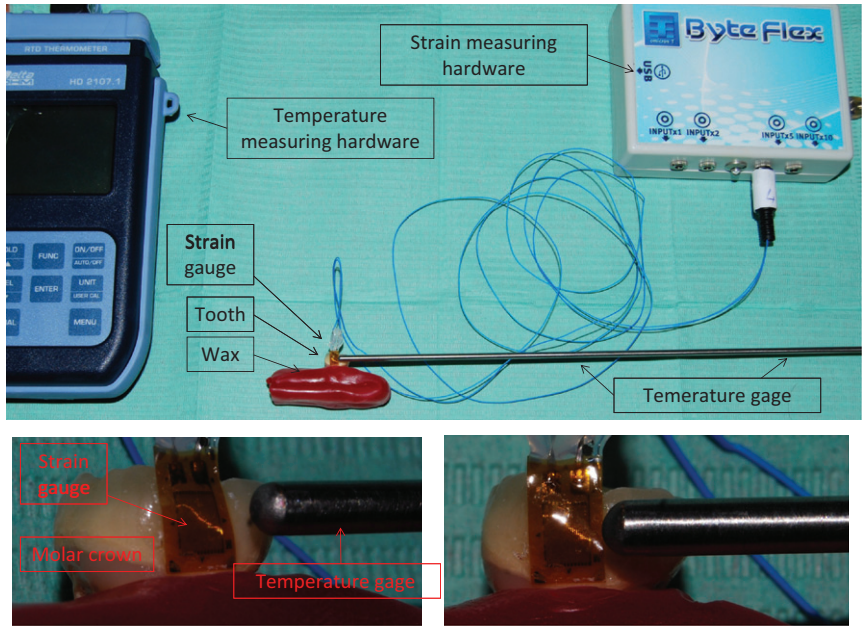

Figure 2. FE model validation process. Strain gauge and temperature gage measuring systems setup.

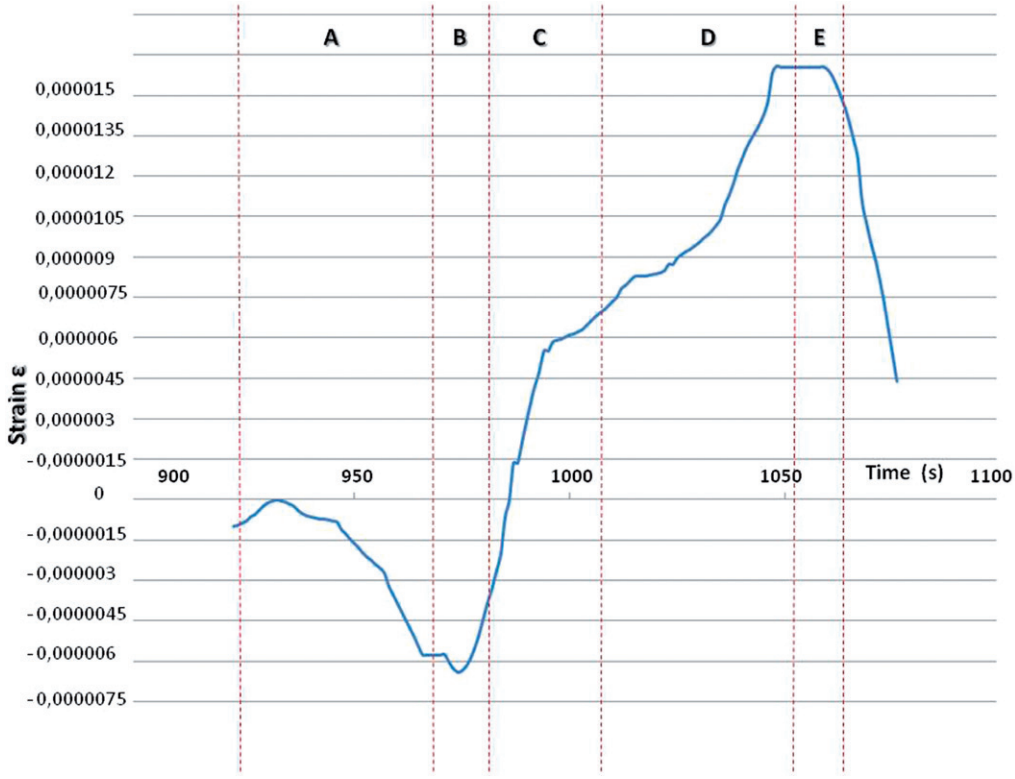

Figure 3. Strain–time function. Dotted lines divide the temperature phases applied to the molar crown.

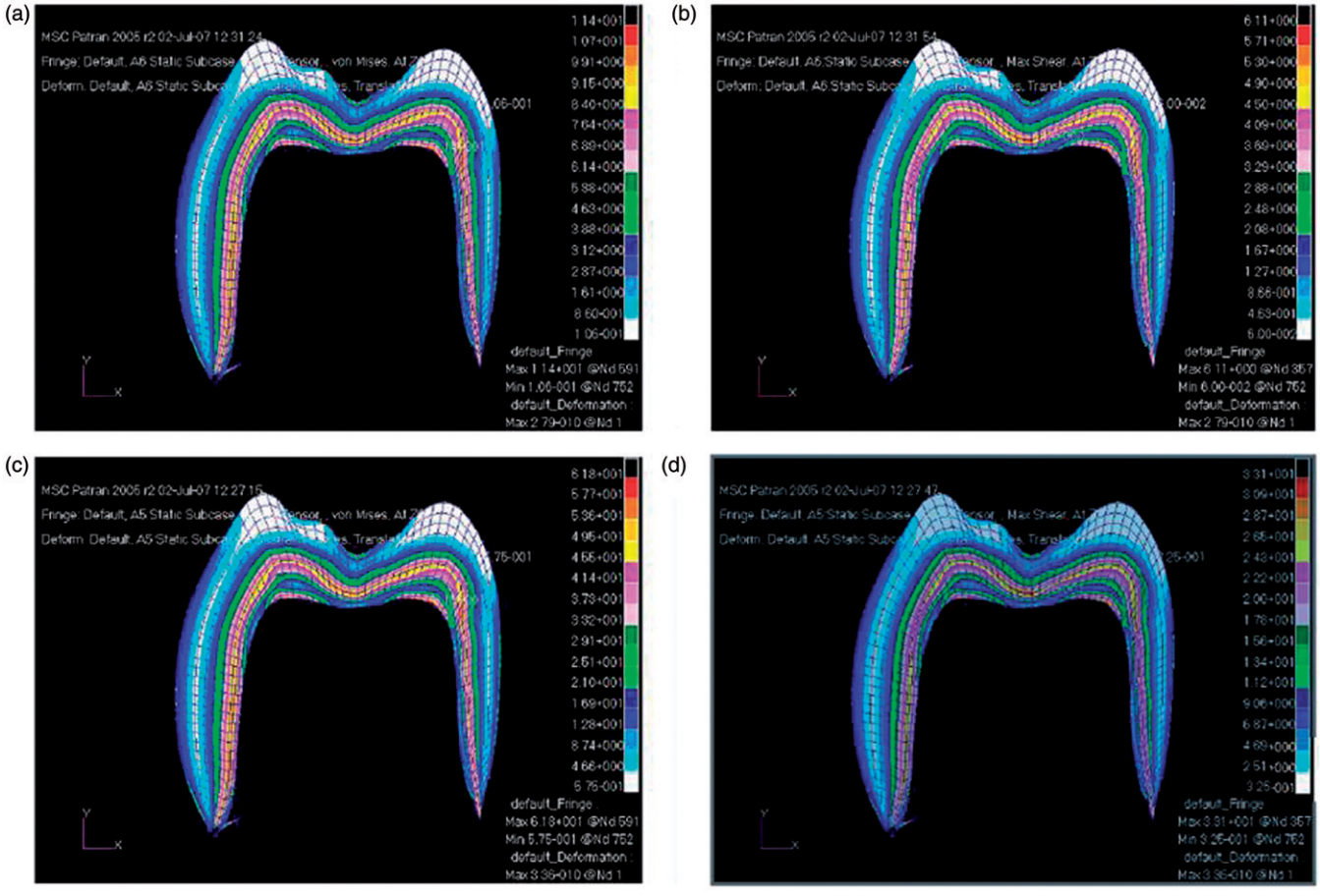

Figure 4. Maximum principal stress values and distribution (a and b) and maximum shear stress values and distribution (b and d) for model 2 Ceramco PFZ (a and c) and model 4 Triceram (b and d) ceramics.

Table 2. Interfacial maximum principal stress (σ-max), ultimate tensile stress of veneer–core interfaces determined by micro-tensile bond strength test (σ-ult), mismatch between core and veneer CETs (Δα) and interfacial maximum shear stress (τ-max).

Model	Veneer material	Δα (με/°C)	σ-max (MPa)	σ-ult (MPa)	% of σ-max to σ-ult	τ-max (MPa)
1	Lava ceram	0.2	0.94	34.3	2	0.5
2	Ceramco pfz	0.2	0.95	75.7	1	0.5
3	Vita vm9	1	5.4	23.5	22	2.9
4	Triceram	1.1	6	45	13	3.2
5	Sakura interaction	0.3	1.5	23.8	6	0.8
6	Zirox	2	11	56.1	19.6	5.9
7	GC initial	0.6	3.2	27.1	11.8	1.7
8	Emax	0.5	2.6	15.1	17.2	1.4

biological structures. With this approach, the more complex 3D FEA can be easily adopted on more restricted populations of ''virtual samples'' still maintaining the virtual statistical approach.

2D model validation

In strain, measuring analysis is important to define the ''undeformed configuration'' of the object being analyzed. Strain state is sensible to environment temperature variations. Thus, the molar crown strain state at room temperature (25 °C) was assumed as undeformed configuration. The 0 strain state reported in Figure 3 correspond to the strain state at room temperature. The linear strain gauge was bonded with its measuring axis parallel to the tooth main axis. In the FE model, this axis corresponds to the *Y* axis. Some principal strains vectors plotting performed during the FE analysis showed that the principal strain direction on the outer surface of the crown is closely parallel to the *Y* axis of the FEA environment. Accordingly, the adopted measuring direction of the strain gauge was considered suitable for model validation. The decreasing temperature (Phase A) produce a shrink of the material being read by the gauge as a strain decreasing in the negative field. The room temperature and the hot air flux (Phases C and D) produce material dilatation and strain state increase from −0.0000075 to 0.000014 ε. This strain range was selected for FE model validation being determined by a temperature variation from 0 °C to 75 °C. The corresponding stress state was calculated according to Equation (1). Thus, the recorded stress was 1.5 MPa (±0.1 MPa), while the FEA-estimated stress value estimated in the same area was 1.67 MPa. Thus the presented 2D model slightly underestimate stress state produced by temperature variation.

FEA-estimated data

The average temperature on teeth surfaces measured not during mastication or swallowing ranged from 30 °C to 35 °C.[36,39] Peak temperatures during chewing and swallowing of hot foods and drinks ranged from 70 °C to 76 °C.[40,41]

The effect of intra-oral peak temperatures on metal-free crowns stress state has still not been addresses.

In the present study, a temperature gradient from 0 °C to 75 °C was applied to the models. The resulting stress state due to thermal dilatations of crown materials has been estimated by finite elements analysis.

Thermal oral environment during function increase the stress state of veneer ceramic and zirconia core due to strain induced by materials thermal expansion. In all the tested models, the higher stress concentrations are estimated along the veneer–core interface (Figure 4). Interfacial stress concentration is determined by the discontinuity between the internal strain state of veneer ceramic and zirconia core. An analogous behavior occurs during fabrication thermo-cycling at high temperatures. However, stress concentrations occurring during fabrication are dissipated due to materials viscoelastic behavior characteristic of the reaction phase transition.

During oral function, the internal stress induced by temperature variation is stored in the system and can generate crack initiation. The veneer–core interface is the weakest point of the system. Accordingly, different studies in literature were addressed to estimate the interfacial strength of porcelain veneers and zirconia cores.[2,42,43]

In the present study, maximum principal stress and maximum shear stress had been estimated along the veneer–core interface. Microtensile bond strength tests are performed to measure the ability of a continuous interface between two materials to withstand a tensile stress which direction is normal to the interfacial plane.

Adopting the principal stress analysis theory to describe the interfacial stress state during a microtensile bond strength test (MTBS), the orientation of the maximum principal stress is normal to the interfacial plane. Accordingly, micro-tensile bond strength test output values can be considered as the stress-state values at which the interfacial plane fails under the maximum principal stress that in a MTBS test is normal to the interface.

Among the phenomenological failure criteria, principal stress criterion is considered suitable to study interface failures of brittle materials, since it account for the orientation of the maximum stress with respect to the interfacial plane. Accordingly, FEA-computed data can be easily compared to experimental MTBS data. The maximum stress criterion assumes that an interface fails when the maximum principal stress exceeds the uniaxial tensile strength normal to the interfacial plane. In the present study, interfacial maximum principal stress were calculated by FEA for each of the tested model that represent different combination of porcelain veneer material to yttria-stabilized-zirconia core. The higher values of interfacial maximum principal stress for each of tested model are listed in Table 2. The higher value of interfacial maximum principal stress of each model was compared to the bond strength value experimentally determined on the same combination of materials.

In all the tested models, the temperature variation between 35 °C and 75 °C does not produce maximum principal stresses in the porcelain–veneer to zirconia–core interface that overcome the ultimate tensile strength of the interface.

The higher percentage of interfacial stress with respect to the interfacial strength was estimated for Vita VM9 and Zirox models (Table 2). The lower percentage of interfacial strength was estimated for Ceramco PFZ (Table 2).

According to our results, temperatures characteristic of normal oral function do not represent a dangerous condition to porcelain–veneer zirconia–core interface. Accordingly, delamination or chipping of porcelain veneer from zirconia core observed in clinical cases are more likely determined by functional mechanical loads or a combination of thermal and mechanical loads.

The stress state due to temperature variation should be carefully taken into consideration while studying the effect of mechanical load on zirconia core crown by FEA. Since the interfacial stress state can be increased by temperature variation up to 20% with respect to the relative failure parameter (in this case interface strength).

This means that stress due to mechanical load combined to temperature variation-induced stress can lead porcelain veneer–zirconia core interfaces to failure.

In other words, the interfacial stress state due to temperature variation is not at all dangerous to the interface integrity, but its intensity is clearly not negligible.

Declaration of interest

The authors confirm that there are no known conflicts of interest associated with this publication and there has been no significant financial support for this work that could have influenced its outcome.

References

1. Deng Y, Miranda P, Pajares A, Guiberteau F, Lawn BR. Fracture of ceramic/ceramic/polymer trilayers for biomedical application. J Biomed Mater Res. 2003;67:828–833.
2. Aboushelib M, De Jager N, Kleverlaan C, Feilzer A. Microtensile bond strength of different comoponents of core veneered all-ceramic restorations. Dent Mater. 2005;21:984–991.
3. Kelly JR. Ceramics in restorateve and prosthetic dentistry. Annu Rev Mater Sci. 1997;27:443–468.
4. Lawn BR, Pajares A, Zhang Y, Deng Y, Polack MA, Lloyd IK, Rekow ED, Thompson VP. Materials design in the performance of all-ceramic crowns. Biomaterial. 2004;2004;25:2885–2892.
5. Filser F, Luthy H, Scharer P, Gauckler L. All-ceramic restorations by new direct ceramic maching process (DCM). J Dent Res. 1998; 77:762 [abstract No. 1046].
6. Luthy H, Filser F, Gauckler L, Scharer P. High reliable zirconia bridges by direct ceramic maching process (DCM). J Dent Res. 1998;77:762 [abstract No. 1045].
7. Morena R, Lockwood PE, Fairhurst CW. Fracture toughness of commercial dental porcelains. Dent Mater. 1986;2:55–62.
8. Drummond JL, King TJ, Bapna MS Koperski RD. Mechanical property evaluation of pressable restorative ceramics. Dent Mater. 2000;16:226–233.
9. Cattell MJ, Palumbo RP, Knowles JC, Crarke RL, Samarawickrama DYD. The effect of vennering and heat treatment on the flexural strength of Empress 2 ceramics. J Dent. 2002;30:161–169.
10. Kuroda Y, Shinya A, Matsuda T, Katagiri S. The mechanical properties of the pressable ceramics and its optimal crystallization. J Dent Mater. 2003;22:221–230. (In Japanese).
11. Guazzato M, Albakry M, Ringer SP, Swain MV. Strength, fracture toughness and microstructure of a selection of all-ceramic materials. Part II. Zirconia based dental ceramics. Dent Mater. 2004;20: 449–436.
12. Rizkalla AS, Jones DW. Mechanical properties of commercial high strength ceramic core materials. Dent Mater. 2004;20:207–212.
13. White SN, Miklus VG, McLaren EA, Lang LA, Caputo AA. Flexural strength of a layered zirconia and porcelain dental all-ceramic system. J Prosthet Dent. 2005;94:125–131.
14. Yilmaz H, Aydin C, Gul BE. Flexural strength and fracture toughness of dental core ceramics. J Prosthet Dent. 2007;98: 120–128.
15. Kim JW, Kim JH, Thompson WP, Zhang Y. Sliding contact fatigue damage in layered ceramic structures. J Dent Res. 2007;86: 1046–1050.
16. Pittayachawan P, McDonald A, Petrie A, Knowles JC. The biaxial flexural strength and fatigue property of Lava Y-TZP dental ceramic. Dent Mater. 2007;23:1018–1029.
17. Kanno T, Milleding P, Wenneberg A. Topography, microhardness, and precision of fit on ready-made zirconia abutment before/after sintering process. Clin Implant Den Relat Res. 2007;9:156–165.
18. Fischer J, Stawarczyk B, Tomic M, Strub JR, Hammerle CH. Effect of thermal misfit between different veneering ceramics and zirconia frameworks on in vitro fracture load of single crowns. Dent Mater J. 2007;26:766–772.
19. Raigrodski AJ, Chiche GJ, Potiket N, Hochstedler JL, Mohamed SE, Billiot S, Mercante DE. The efficacy of posterior three-unit zirconium-oxide-based ceramic fixed partial dental prostheses: a prospective clinical pilot study. J Prosthet Dent. 2006;96:237–244.
20. Sailer I, Feher A, Filser F, Gauckler LJ, Luthy H, Hammerle CHF. Five-year clinical recults of zirconia frameworks for posterior fixed partial dentures. Int J Prosthodont. 2007;20:383–388.
21. Juvinall RC, Marshek KM. Fundamentals of machine component design, 2nd ed. New York: Wiley; 1991.
22. Guazzato M, Albakry M, Ringer SP, Swain MV. Strength, fracture toughness and microstructure of a selection of all-ceramic materials. Part I. Zirconia based dental ceramics. Dent Mater. 2004;20: 440–456.
23. Filser F, Kocher P, Weibul F, Luthy H, Scharer P, Gauckler LJ. Reliability and strength of all-ceramic dental restorations fabricated by direct ceramic machining (DCM). Int J Comp Dent. 2001;4: 89–106.
24. Luthy H, Filser F, Loeffel O, Schuhmacher M, Gauckler LJ, Hammerle CHF. Strength and reliability of four unit all-ceramic posterior bridges. Dent Mater. 2005;21:930–937.
25. Marrelli M, Maletta C, Inchingolo F, Alfano M, Tatullo M. Three-point bending tests of zirconia core/veneer ceramics for dental restorations. Int J Dent. 2013;2013:831976.
26. Piconi C, Maccauro G. Zirconia as a ceramic biomaterial. Biomaterials. 1999;20:1–25.
27. Covacci V, Bruzzese N, Maccauro G, Andreassi C, Ricci GA, Piconi C, Marmo E, Burger W, Cittadini A. In vitro evaluation of the mutagenic and carcinogenic power of high purity zirconia ceramic. Biomaterials. 1999;20:371–376.
28. Rinke S, Schäfer S, Lange K, Gersdorff N, Roediger M. Practice-based clinical evaluation of metal-ceramic and zirconia molar crowns: 3-year results. J Oral Rehabil. 2013;40:228–237.
29. Raigrodski AJ, Hillstead MB, Meng GK, Chung KH. Survival and complications of zirconia-based fixed dental prostheses: a systematic review. J Prosthet Dent. 2012;107:170–177.
30. Teng J, Wang H, Liao Y, Liang X. Evaluation of a conditioning method to improve core-veneer bond strength of zirconia restorations. J Prosthet Dent. 2012;107:380–387.
31. Poggio CE, Dosoli R, Ercoli C. A retrospective analysis of 102 zirconia single crowns with knife-edge margins. J Prosthet Dent. 2012;107:316–321.
32. Al-Dohan HM, Yaman P, Dennison JB, Razzog ME, Lang BR. Shear strength of core-veneer interface in bi-layered ceramics. J Prosthet Dent. 2004;91:349–355.
33. Kelly JR, Tesk JA, Sorensen JA. Failure of all-ceramic fixed partial dentures in vitro and in vivo: analysis and modeling. J Dent Res. 1995;74:1253–1258.
34. Kirmali O, Akin H, Ozdemir AK. Shear bond strength of veneering ceramic to zirconia core after different surface treatments. Photomed Laser Surg. 2013;31:261–268.
35. Zhang Z, Zhou S, Li Q, Li W, Swain MV. Sensitivity analysis of bi-layered ceramic dental restorations. Dent Mater. 2012;28:e6–e14.
36. Zhang Z, Guazzato M, Sornsuwan T, Scherrer SS, Rungsiyakull C, Li W, Swain MV, Li Q. Thermally induced fracture for core-veneered dental ceramic structures. Acta Biomater. 2013;9: 8394–8402.
37. Mainjot AK, Schajer GS, Vanheusden AJ, Sadoun MJ. Influence of veneer thickness on residual stress profile in veneering ceramic: measurement by hole-drilling. Dent Mater. 2012;28:160–167.
38. Mainjot AK, Schajer GS, Vanheusden AJ, Sadoun MJ. Residual stress measurement in veneering ceramic by hole-drilling. Dent Mater. 2011;27:439–444.

39. Ernst CP, Canbek K, Euler T, Willershausen B. In vivo validationof historical in vitro thermocycling temperature range for dental material testing. Clin Oral Investig. 2004;8:130–138.
40. Spierings TA, Peters MC, Plasschaert AJ. Surface Temperature of oral tissues. A review. J Biol Buccale. 1984;12:91–99.
41. Feuerstein O, Zeichner, Imbari C, Ormianer Z, Samet N, Weiss EI. Temperature changes in dental implants following exposure to hot substances in an ex vivo model. Clin Oral Implants Res. 2008;19: 629–633.
42. Barcley CW, Spence D, Laird WR. Intra-oral temperatures during function. J Oral Rehabil. 2005;32:886–894.
43. Fazi G, Vichi A, Ferrari M. Microtensile bond strength of three different veneering porcelain systems to a zirconia core for all ceramic restorations. Am J Dent. 2010;23:347–350.